Neurobiology of Disease 121 (2019) 263–273

Contents lists available at ScienceDirect

Neurobiology of Disease

journal homepage: www.elsevier.com/locate/ynbdi

Pharmacological enhancement of retinoid-related orphan receptor α function mitigates spinocerebellar ataxia type 3 pathology

Masashi Watanave[a], Chiaki Hoshino[a], Ayumu Konno[a], Yumi Fukuzaki[a], Yasunori Matsuzaki[a], Tohru Ishitani[b], Hirokazu Hirai[a,*]

[a] Department of Neurophysiology & Neural Repair, Gunma University Graduate School of Medicine, Maebashi, Gunma 371-8511, Japan
[b] Institute for Molecular & Cellular Regulation, Gunma University, Maebashi, Gunma 371-8511, Japan

ARTICLE INFO

Keywords:
Cerebellum
Purkinje cell
Spinocerebellar ataxia type 3
Machado–Joseph disease
AAV vector
Retinoid-related orphan receptor alpha
Type 1 metabotropic glutamate receptor
Slow excitatory postsynaptic current

ABSTRACT

Cerebellar Purkinje cells (PCs) are the sole output neurons of the cerebellar cortex, and damage to PCs results in motor deficits. Spinocerebellar ataxia type 3 (SCA3, also known as Machado–Joseph disease), a hereditary neurodegenerative disease, is caused by an abnormal expansion of the polyglutamine tract in the causative ATXN3 protein. SCA3 affects a wide range of cells in the central nervous system, including those in the cerebellum. To unravel SCA3 pathology, we used adeno-associated virus serotype 9 (AAV9) vectors to express full-length ATXN3 with an abnormally expanded 89 polyglutamine stretch (ATXN3[Q89]) in cerebellar neurons of mature wild-type mice. Mice expressing ATXN3[Q89] exhibited motor impairment in a manner dependent on the viral titer. Immunohistochemistry of the cerebellum showed ubiquitinated nuclear aggregates in PCs; degeneration of PC dendrites; and a significant decrease in multiple proteins including retinoid-related orphan receptor α (RORα), a transcription factor, and type 1 metabotropic glutamate receptor (mGluR1) signaling molecules. Patch clamp analysis of ATXN3[Q89]-expressing PCs revealed marked defects in mGluR1 signaling. Notably, the emergence of behavioral, morphological, and functional defects was inhibited by a single injection of SR1078, an RORα/γ agonist. These results suggest that RORα plays a key role in mutant ATXN3-mediated aberrant phenotypes and that the pharmacological enhancement of RORα could function as a method for therapeutic intervention in SCA3.

1. Introduction

Retinoid-related orphan receptor α (RORα) is a transcription factor that is abundantly expressed in cerebellar Purkinje cells (PCs) and plays a critical role in cerebellar development, especially in the dendritic differentiation of PCs. The *staggerer* mutant, which is the classical mouse model for ataxia, is deficient for RORα function (Hamilton et al., 1996; Sidman et al., 1962). These mice show aberrant development of the cerebellum, and their PCs show rudimentary dendritic arbors along with the absence of mGluR signaling (Boukhtouche et al., 2006; Iizuka et al., 2016; Mitsumura et al., 2011).

Spinocerebellar ataxia type 1 (SCA1) and type 3 (SCA3, also known as Machado–Joseph disease) are hereditary neurodegenerative diseases for which there is no cure. They are caused by an abnormal expansion of CAG repeats present in coding regions of responsible genes, *ATXN1* and *ATXN3*, respectively, resulting in production of mutant ATXN1 and

Abbreviations: AAV9, adeno-associated virus serotype 9; AMPAR, α-amino-3-hydroxy-5-methyl-4-isoxazole-propionate receptor; ATXN3[Q15], human Ataxin-3 with 15 glutamine repeats; ATXN3[Q89], human Ataxin-3 with 89 glutamine repeats; C57BL/6 mice, C57 black 6 mice; Cm, membrane capacitance; CNS, central nervous system; CPCCOEt, 7-hydroxyiminocyclopropan[*b*]chromen-1a-carboxylate ethyl ester; GluD2, ionotropic glutamate receptor delta 2 subunit; EPSC, excitatory post synaptic current; GFP, green fluorescent protein; HA, hemagglutinin; ISI, inter-stimulus interval; IP_3R1, inositol 1,4,5-triphosphate receptor type 1; LTD, long-term depression; mGluR1, metabotropic glutamate receptor type 1; NBQX, 2,3-dioxo- 6-nitro-1,2,3,4-tetrahydrobenzo[*f*]quinoxaline-7-sulfonamide; P, postnatal day; P2A, 2A peptide derived from porcine teschovirus-1; pA, polyadenylation; PAM, positive allosteric modulator; PBS, phosphate-buffered saline; PC, Purkinje cell; PF, parallel fiber; PKC, protein kinase C; PNS, peripheral nervous system; PPF, paired-pulse facilitation; RT-PCR, reverse transcription polymerase chain reaction; Ro0711401, 9H-xanthene-9-carboxylic acid (trifluomethyl-oxazol-2-yl) amide; RORα, retinoid-related orphan receptor α; rSynI-minCMV, rat synapsin I promoter with a minimal cytomegalovirus sequence; SCA1, spinocerebellar ataxia type 1; SCA3, spinocerebellar ataxia type 3; SR1078, n-[4-[2,2,2-trifluoro-1-hydroxy-1-(trifluoromethyl)ethyl]phenyl]-4-(trifluoromethyl)benzamide; TRPC3, transient receptor potential cation channel type 3; UIM, ubiquitin-interacting motif; WPRE, woodchuck hepatitis virus posttranscriptional regulatory element

* Corresponding author.
E-mail address: hirai@gunma-u.ac.jp (H. Hirai).

https://doi.org/10.1016/j.nbd.2018.10.014
Received 14 June 2018; Received in revised form 26 September 2018; Accepted 17 October 2018
Available online 19 October 2018
0969-9961/

ATXN3 proteins with an abnormally expanded polyglutamine stretch (Kawaguchi et al., 1994; Orr et al., 1993; Yamada et al., 2008). Both SCA1 and SCA3 are characterized by wide spread neurodegeneration in the central nervous system (CNS) and peripheral nervous system (PNS) (Mieda et al., 2016; Suto et al., 2016; Takechi et al., 2013). The resulting deficits include progressive cerebellar ataxia and variable additional symptoms including visual problems, dysarthria and dysphagia (Globas et al., 2008). Using the mouse model of SCA1, a previous study showed that ATXN1 and RORα form a transcriptional complex via Tip60 (Serra et al., 2006). An abnormal expansion of polyglutamine in ATXN1 disrupts the formation of this complex, leading to the degradation of RORα (Hirai and Kano, 2018; Serra et al., 2006). Recently, we showed that the PCs of SCA1 mice have attenuated mGluR signaling, and that potentiation of mGluR signaling by baclofen, an agonist of $GABA_B$ receptor closely associated with mGluR1, significantly restored the behavioral phenotype (Shuvaev et al., 2017). Thus, SCA1 mice share a similar pathology with the *staggerer* mutant mice in terms of RORα deficiency and disruption of mGluR signaling (Hirai and Kano, 2018).

Similar to *staggerer*, we have shown a significant reduction in RORα and aberrant mGluR signaling in the SCA3 model mice that expressed a truncated ATXN3 protein with an abnormally expanded polyglutamine (Konno et al., 2014). These results suggest that RORα deficiency and disruption of mGluR1 signaling are critical to the generation of the pathology shared between SCA1 and SCA3. However, the SCA3 model mice that we used expressed an ATXN3 protein that comprises of only the polyglutamine stretch and the 17 amino acids of the C-terminal of the protein (Torashima et al., 2008) (Fig. 1A). The deleted N-terminal portion included 286 amino-acid residues which contained the catalytic Josephin domain and 2 ubiquitin interacting motifs (Li et al., 2015). The truncated ATXN3 protein with an abnormally expanded polyglutamine is shown to be more toxic compared to the full length ATXN3 with a similar length of the polyglutamine tract (Ikeda et al., 1996). Thus, pathogenesis seen in PCs of SCA3 transgenic mice (Konno et al., 2014) may potentially differ from that of SCA3 patients. To verify if this is indeed the case, and to further dissect SCA3 pathology, we used adeno-associated virus serotype 9 (AAV9) vectors to express a full length ATXN3 protein with an abnormally expanded 89 polyglutamine stretch (Q89) in the mature cerebellum of wild-type mice, and examined the influence of this protein on RORα and mGluR signaling in PCs.

2. Materials and methods

2.1. Animals

Wild-type C57BL/6 mice were used in this study. All procedures for the care and treatment of animals were performed according to the Japanese Act on the Welfare and Management of Animals, and the Guidelines for Proper Conduct of Animal Experiments as issued by the Science Council of Japan. The experimental protocol was approved by the Institutional Committee of Gunma University (No. 17-026; 17-034). All efforts were made to minimize suffering and to reduce the number of animals that were used.

2.2. Drugs

A mGluR1 positive allosteric modulator (PAM), Ro0711401 [9H-xanthene-9-carboxylic acid (trifluomethyl-oxazol-2-yl) amide] (Notartomaso et al., 2013), was purchased from Aquila Pharmatech LLC (Waterville, OH, USA), and administered subcutaneously [10 mg/kg body weight (BW)]. A synthetic RORα/γ agonist, SR1078 (Wang et al., 2010), was obtained from R&D systems (Cat. No. 4874, Minneapolis, MN, USA) and administered by intraperitoneal injection (10 mg/kg BW).

2.3. Construction and production of AAV vectors

The AAV9 expression plasmids (pAAV/rSynI-minCMV-GFP-P2A-HA-ATXN3[Q89 or Q15]-WPRE) (Fig. 1A) were constructed based on pAAV/rSynI-minCMV-GFP-WPRE (Huda et al., 2014). GFP was substituted with GFP-P2A-(*Not*I), which was digested out from pCL20c/rSynI(1.0)-minCMV-GFP-P2A-(*Not*I)-WPRE (Matsuzaki et al., 2014) using 2 restriction enzymes, *Age*I and *Not*I. The resulting plasmid, pAAV/SynI-minCMV-GFP-P2A-(*Not*I)-WPRE, was used for the insertion of HA-tagged full-length human ATXN3 cDNA containing 89 or 15 CAG repeats at the *Not*I site. The CAG repeat length in human ATXN3 cDNA was artificially expanded to 89 repeats using PCR-based trinucleotide repeat expansion (Laccone et al., 1999). The AAV-PHP.B (Deverman et al., 2016) expression plasmids (pAAV/CBh-GFP-P2A-HA-ATXN3[Q89 or Q15]-WPRE) (Supplementary Fig. 1A) were created by the substitution of SynI-minCMV promoter in pAAV/rSynI-minCMV-GFP-P2A-HA-ATXN3[Q89 or Q15]-WPRE by a CBh promoter (Gray et al., 2011) using 2 restriction enzymes (*Xho*I and *Age*I).

Recombinant single-strand AAV9 and AAV-PHP.B vectors were generated by the co-transfection of HEK293T cells with 3 plasmids: the expression plasmid containing ATXN3, pHelper (Stratagene, La Jolla, CA, USA), and pAAV2/9 (kindly provided by Dr. J. Wilson) or pAAV-PHP.B (Matsuzaki et al., 2018). The viral particles were purified using ammonium sulfate precipitation and iodixanol continuous gradient centrifugation as described previously (Miyake et al., 2012). Genomic titers of the purified AAV9 vectors were determined by a real-time quantitative PCR using THUNDERBIRD SYBR qPCR Mix (Toyobo, Osaka, Japan) along with the primers 5′-CTGTTGGGCACTGACAA TTC-3′ and 5′-GAAGGGACGTAGCAGAAGGA-3′, which targeted the woodchuck hepatitis virus post-transcriptional regulatory element (WPRE) sequence. The expression plasmid vectors were used as standards. The viral titers obtained were 7.9×10^{13} vector genomes (vg)/ml (AAV9-ATXN3[Q15]), 1.7×10^{14} vg/ml (AAV9-ATXN3[Q89]), 1.8×10^{13} vg/ml (PHP.B-ATXN3[Q15]), and 1.4×10^{13} vg/ml (PHP.B-ATXN3[Q89]).

2.4. Viral injection

The AAV9 vector was injected directly into the cerebellar tissue. After inducing deep anesthesia via an intraperitoneal injection of ketamine (100 mg/kg BW) and xylazine (10 mg/kg BW), postnatal day (P) 35–36 old mice were placed in a stereotactic frame. The skin covering the occipital bone was cut, and a burr hole was made 7 mm caudal from the bregma. The tip of a Hamilton syringe (33 gauge) with an attached micropump [UltraMicroPump II; World Precision Instrument (WPI) Sarasota, FL, USA] was inserted 1.8 mm below the pia mater of the cerebellar vermis. Ten microliters of viral solution (1×10^{11} vg or 3×10^{11} vg) or phosphate-buffered saline (PBS) was injected at a rate of 400 nl/min using microprocessor-based controller (Micro4; WPI). AAV-PHP.B was intravenously administrated. The AAV-PHP.B vectors were loaded into a 29-gauge syringe (SS-10M2913A, TERUMO, Tokyo, Japan). The deeply anesthetized mice were placed on their left side, and the facial skin was stretched to immobilize the face during the injection. The needle was inserted into the right orbit along the medial angle of the right eye until the tip reached the orbital bone where the orbital venous plexus is located. Furthermore, 100 µl of the viral solution was injected during 1 min.

2.5. Immunohistochemistry

Three weeks after injection with the AAV9 vectors, mice were deeply anesthetized and perfused intracardially with 4% paraformaldehyde in 0.1 M phosphate buffer (pH 7.4). The entire brain was removed and immersed in 4% paraformaldehyde in 0.1 M phosphate buffer overnight at 4 °C. Parasagittal cerebellar slices (50 µm thick) were prepared using a vibratome (VT1000S, Leica, Wetzlar, Germany).

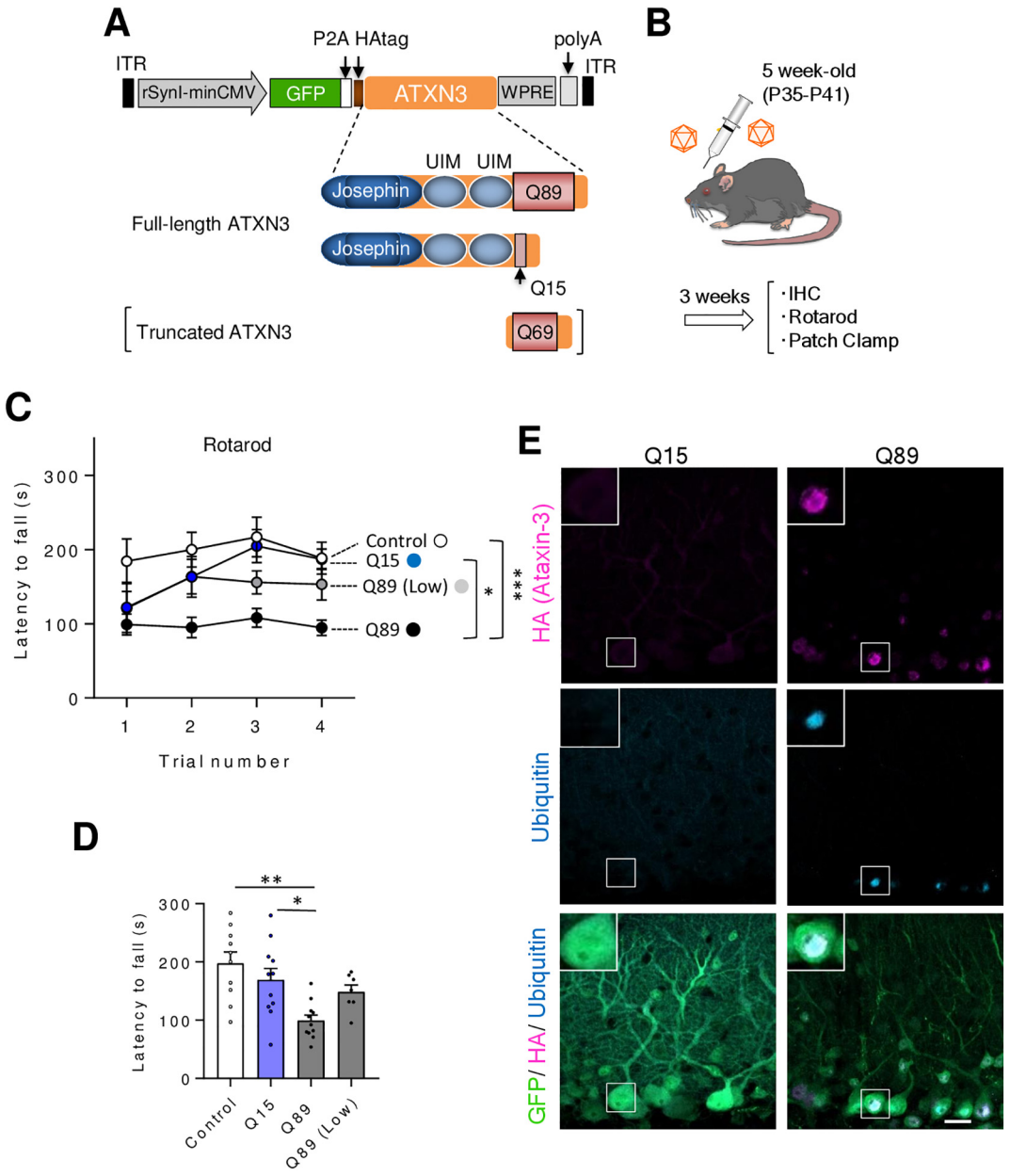

Fig. 1. Titer-dependent motor deficit in mice injected with a AAV vector expressing ATXN3[Q89]. (A) Scheme depicting the expression cassettes of the AAV vector plasmids. GFP-P2A-HA-tagged full-length ATXN3[Q89] or ATXN3[Q15] were expressed under the control of the neuron-specific rSynI-minCMV promoter. P2A, a "self-cleaving" peptide sequence, was inserted between GFP and HA-ATXN3. A WPRE sequence was placed downstream of the ATXN3 gene to enhance the mRNA stabilization. Full-length ATXN3 is composed of the N-terminal catalytic Josephin domain and 2 UIMs in addition to subsequent polyglutamine tract. Composition of the truncated ATXN3 gene previously used for the generation of the SCA3 transgenic mice (Torashima et al., 2008) is presented for comparison. (B) Schematic of the experimental plan. P35–41 wild-type mice received injection of AAV9 vectors, and analyzed 3 weeks post-injection by rotarod, immunohistochemistry (IHC) and patch clamp. (C) Results of the rotarod test, with acceleration from 4 to 40 rpm over 5 min. Mice were placed on the rod and latency to fall was measured 4 times with 30-min intervals between trials. We examined mice which received PBS injection (control) and those virally expressing ATXN[Q15] (Q15) (3×10^{11} vg) or ATXN3[Q89] (Q89) (Low: 1×10^{11} vg or 3×10^{11} vg) (control: 10 mice, Q15: 11 mice, Q89: 11 mice, Q89 (Low); 7 mice). (D) Graph showing average time taken in 4 trials of the rotarod test. (E) Immunohistochemistry of the cerebellar cortex expressing ATXN3[Q15] (Q15) or ATXN3[Q89] (Q89). Sagittal sections triple immunolabeled for HA (magenta), ubiquitin (light blue) and GFP (green) were examined by a confocal microscopy. Scale bar 20 μm. Asterisks indicate statistically significant differences as determined by one-way ANOVA followed by Bonferroni's post hoc test. *P < .05, **P < .01, ***P < .001. HA; hemagglutinin, rSynI-minCMV; rat synapsin I promoter with a minimal cytomegalovirus sequence, P; postnatal day, P2A; 2A peptide derived from porcine teschovirus-1, pA; polyadenylation, PBS; phosphate-buffered saline, UIM; ubiquitin-interacting motif, WPRE; woodchuck hepatitis virus posttranscriptional regulatory element. (For interpretation of the references to colour in this figure legend, the reader is referred to the web version of this article.)

The tissue slices were permeabilized, blocked with PBS containing 5% (v/v) normal donkey serum, 0.5% (v/v) Triton X-100, and 0.05% NaN_3 (blocking solution), and treated overnight at 4 °C in blocking solution that contained the following antibodies: rat polyclonal anti-GFP (1:1000; GFP-Rb-Af2020; Frontier Institute, Hokkaido, Japan), goat polyclonal anti-RORα (1:400; sc-6062; Santa Cruz Biotechnology, Dallas, TX, USA), or mouse monoclonal anti-calbindin D-28 k (1:1000, Swant, Bellinzona, Switzerland). After washing twice with PBS containing 0.5% Triton X-100, and 4 times with PBS containing 0.1% Triton X-100 at room temperature (23 °C), the slices were incubated overnight at 4 °C in the blocking solution with the following secondary antibodies (1:1000; all purchased from Thermo Fisher Scientific,

Waltham, MA, USA): Alexa Fluor 488-conjugated donkey anti-rat IgG, Alexa Fluor 568-conjugated donkey anti-goat IgG and Alexa Fluor 647-conjugated donkey anti-mouse IgG. After washing 3 times with PBS at room temperature (23 °C), the slices were mounted on glass slides with ProLong Gold/Diamond Antifade Reagent (Thermo Fisher Scientific). Each specimen was observed with a fluorescent microscope (BZ-X700; Keyence, Osaka, Japan) or a confocal laser-scanning microscope (LSM 800, Carl Zeiss, Oberkochen, Germany). The following primary antibodies were used in this study: rat polyclonal anti-GFP (1:1000; GFP-Rb-Af2020; Frontier Institute, Hokkaido, Japan), goat polyclonal anti-RORα (1:400; sc-6062; Santa Cruz Biotechnology, Dallas, TX, USA; or rabbit polyclonal anti-RORα [1:100; SAB2102040; Sigma-Aldrich, St Louis, MO, USA]; Supplementary Fig. 1), mouse monoclonal anti-calbindin D-28 k (1:1000, Swant, Bellinzona, Switzerland), mouse monoclonal anti-GFP (1:1000; GTX21218; GeneTex, Irvine, CA, USA), rat monoclonal anti-HA (1:1000; 3F10; Roche, Basel Switzerland), and rabbit monoclonal anti-ubiquitin (Lys48 specific; 1:200; 05–1307; Millipore, Darmstadt, Germany). The appropriate secondary antibodies were selected from those as follows (1:1000; all purchased from Thermo Fisher Scientific, Waltham, MA, USA): Alexa Fluor 488-conjugated donkey anti-rat IgG, Alexa Fluor 488-conjugated donkey anti-mouse, IgG Alexa Fluor 568-conjugated donkey anti-goat IgG, IgG Alexa Fluor 568-conjugated donkey anti-rat IgG, IgG Alexa Fluor 568-conjugated donkey anti-rabbit IgG, Alexa Fluor 647-conjugated donkey anti-mouse IgG and Alexa Fluor 647-conjugated donkey anti-rabbit IgG.

To quantify RORα in PCs, RORα immunoreactive intensity was measured in PC nuclei present in the parasagittal sections of cerebellar vermis. Fluorescence images of stained sections were captured using a confocal microscope (LSM 800), ensuring that the signal intensity was below the saturation level. Subsequently, the outlines of the PC nuclei were traced, and the fluorescence intensity in the enclosed areas was measured using Fiji (ImageJ; https://fiji.sc/).

2.6. Quantitative reverse transcription polymerase chain reaction (RT-PCR)

Parasagittal cerebellar slices were prepared from mice 21–26 days after AAV injection, and homogenized using BioMasher II (320103, nippi, Tokyo, Japan) with PowerMasher II (891300, nippi) in TRIzol Reagent (Life Technologies, Carlsbad, CA, USA) and frozen rapidly in liquid nitrogen. After thawing at 37 °C, total RNAs were isolated using RNeasy Mini Kit (QIAGEN, Hilden, Germany) and stored at −80 °C. Reverse transcription was performed using ReverTra Ace qPCR RT Master Mix with gDNA Remover (Toyobo, Osaka, Japan) to synthesize cDNA from the cerebellar RNA samples, and quantitative PCR was performed using KAPA SYBR Fast qPCR Kit (NIPPON Genetics, Tokyo, Japan). The forward (F) and reverse (R) primers used had the following sequences; Gapdh-F: GTGTTCCTACCCCCAATGTG, Gapdh-R: GGTGGA AGAGTGGGAGTTGCTG, EGFP-F: CTGGGGCACAAGCTGGAGTACAAC, EGFP-R: GTGTTCTGCTGGTAGTGGTCG, Rora-F: CCAGAACATATCCA AATCCCACC, Rora-R: GCTTCTGTAATCTTGATGGCAC, mGluR1-F: TGCACCTGGAAGGTATGACA, mGluR1-R: CACTTCCCCTTTCCGTA TGA, Trpc3-F: TGGATTGCACCTTGTAGCAG, Trpc3-R: ACGTGAACTG GGTGGTCTTC, Itpr1-F: GAAGCAGCATGTGTTCCTGA, Itpr1-R: GGTCT ACCTCTGCAGCCAAG. The thermal cycling program used had an initial denaturation step of 95 °C for 30 s, followed by 40 cycles at 95 °C for 5 s and at 60 °C for 60 s.

2.7. Western blotting

Samples from brain block tissues of the cerebellum were homogenized with a lysis buffer (0.2 M PB and 2% sodium dodecyl sulfate). Protein concentration was determined by micro BCA assay (Thermo Fisher Scientific). Homogenates were adjusted to 1 mg/ml by using lysis buffer and sample buffer (Bio-Rad, Hercules, CA, USA). Samples (10 μl) were loaded and separated by 4–20% Mini-PROTEAN TGX Precast Protein Gels (Bio-Rad) electrophoresis and transferred to PVDF transfer membranes (Trans-Blot Turbo Transfer Pack, Bio-Rad). Membranes were blocked with a blocking solution (PVDF Blocking Reagent for Can Get Signal, Toyobo) at 4 °C overnight. After washing with 20 mM Tris, 500 mM NaCl, 0.05% Tween 20 (TBS-T), the membranes were incubated with primary antibodies: rabbit anti-mGluR1 (1:2000; Af811; Frontier Institute), rabbit anti-RORa (1:1000; LS-A5539; LSBio, Seattle, DC, USA), rabbit anti-IP_3R1 (1:2000; Af860; Frontier Institute), rabbit anti-TRPC3 (1:2000; ACC-016; Alomone labs, Jerusalem, Israel), rabbit anti-GluD2 (1:2000; AB_2571600; Frontier Institute), rabbit anti-GFP (1:1000; Af2020; Frontier Institute), and mouse anti-β-Actin (1:5000; A1978 Sigma Aldrich) diluted in the primary solution (Can Get Signal Immunoreaction Enhancer Solution 1, Toyobo) for 2 h at room temperature. Following washing with TBS-T, the membranes were incubated with secondary antibodies: HRP-conjugated anti-rabbit IgG (1:30,000; Santa Cruz Biotechnology) and HRP-conjugated anti-mouse IgG (1:10,000; Santa Cruz Biotechnology) diluted in the secondary solution (Can Get Signal Immunoreaction Enhancer Solution 2, Toyobo) for 2 h at room temperature. After washing with TBS-T and TBS, the immunoblots were detected by chemiluminescence (Clarity Western ECL Substrate, Bio-Rad) with an imaging system (Quantity one, Bio-Rad). The optical density of protein bands was quantified using the gel analysis function of NIH Image J software (https://imagej.nih.gov/ij/).

2.8. Immunoprecipitation

Proteins from cell extracts obtained from the cerebellar vermis were immunoprecipitated with control IgG or anti-HA antibody and protein G-Sepharose (GE Healthcare, Uppsala, Sweden). For immunoblotting, immunoprecipitates or whole cell extracts were resolved by sodium dodecyl sulfate-polyacrylamide gel electrophoresis and transferred onto polyvinylidene fluoride membranes (GE Healthcare, Buckinghamshire, UK). Membranes were immunoblotted with anti-HA or anti RORα antibodies, and the bound antibodies were visualized with horseradish-peroxidase-conjugated antibodies against rabbit or mouse IgG (EMD Chemicals Inc., Darmstadt, Germany) using the ChemiLumi-One L Chemiluminescent Kit (Nacalai Tesque).

2.9. Patch clamp recording

Parasagittal cerebellar slices (250 μm in thickness) were prepared from mice 21–26 days after AAV vector injection. Briefly, mice were anesthetized deeply with inhalation of isoflurane (3%) and killed by decapitation. The whole brain was quickly dissected out and immersed for a couple of minutes in an ice-cold solution containing the following (in mM): 234 sucrose, 26 $NaHCO_3$, 2.5 KCl, 1.25 NaH_2PO_4, 11 glucose, 10 $MgSO_4$, 0.5 $CaCl_2$ (pH 7.4 when bubbled with 95% O_2 and 5% CO_2). Parasagittal slices of the cerebellar vermis were obtained using a microslicer (ZERO1; Dosaka-EM, Kyoto, Japan). The slices were maintained in an extracellular solution containing (in mM): 125 NaCl, 2.5 KCl, 2 $CaCl_2$, 1 $MgCl_2$, 1.25 NaH_2PO_4, 26 $NaHCO_3$, 10 D-glucose, and 0.1 picrotoxin, bubbled continuously with a mixture of 95% O_2 and 5% CO_2 at room temperature for at least 1 h before commencing recording. PCs were visualized using a 40× water-immersion objective attached to an upright microscope (Axioskop; Carl Zeiss). All whole-cell recordings were made from PCs at room temperature (26 °C) and the slices were continuously perfused with the extracellular solution during the experiment. The resistance of patch pipettes was 3–6 MΩ when filled with intracellular solution containing (in mM): 122.5 Cs methane sulfonate, 17.5 CsCl, 8 NaCl, 2 MgATP, 0.3 NaGTP, 10 Hepes, 0.2 EGTA and 5 sucrose (pH 7.2, adjusted with CsOH).

Stimulation pipettes were filled with the extracellular solution and placed in the molecular layer to activate parallel fibers (PFs). The holding potential of PCs was −70 mV. Liquid junction potentials were not corrected. To estimate passive electrical properties of the recorded PCs, we applied 10 mV hyperpolarizing voltage pulses (from −70 mV to −80 mV, 200 ms duration). The averaged trace of 10 current

responses was used for the parameter estimation. Membrane capacitance and input resistance were calculated from the integral of the capacitive charging current, and from the steady-state current amplitude measured late during the pulse, respectively.

Selective stimulation of PFs was confirmed by paired-pulse facilitation (PPF) of EPSC amplitudes with a 50 ms inter-stimulus interval (ISI) and the graded nature of the evoked EPSC amplitudes with stimulus intensity. To isolate mGluR1-mediated slow EPSCs, repetitive PF stimuli (100 Hz) were applied in the presence of 20 μM 2,3-dioxo-6-nitro-1,2,3,4-tetrahydrobenzo[*f*]quinoxaline-7-sulfonamide (NBQX), a highly selective competitive antagonist of AMPA-type glutamate receptors (Libbey et al., 2016).

2.10. Biocytin infusion to PCs and immunohistochemistry

For visualization of PC morphology, 0.5% biocytin (Sigma-Aldrich, St Louis, MO, USA) was diluted with the intra- cellular solution and infused by passive diffusion through a patch pipette into whole cell-clamped PCs. Cerebellar slices were then fixed with 4% paraformaldehyde. After overnight fixation at 4 °C, the slices were rinsed in PBS adjusted to pH 7.4 (3 times, 5 min each), permeabilized and blocked with PBS containing 2% (v/v) normal donkey serum, 0.1% (v/v) TritonX-100 and 0.05% NaN_3 (blocking solution). The slices were then rinsed in PBS, pH 7.4 (3 times, 5 min each), and treated with streptavidin-conjugated Alexa 594 (2 μg/ml, Thermo Fisher Scientific) for 2 h at room temperature (23 °C). PC morphology was analyzed using a confocal laser-scanning microscope (LSM800).

2.11. Rotarod test

The motor control ability of mice was evaluated by a rotarod test (MK-610A/RKZ; Muromachi Kikai, Tokyo, Japan). Mice were subjected to 4 trials separated by 30-min intervals on the rod while accelerating from 4 to 40 rpm in 5 min. The rotarod tests were conducted at 3 weeks after AAV vector injection.

2.12. Statistical analyses

Significant differences were analyzed via Welch test, Bonferroni post hoc test after a one-way analysis of variance (ANOVA), and repeated measures ANOVA using GraphPad Prism 5 (GraphPad Software, San Diego, CA, USA). The data are expressed as the mean ± standard error of mean.

3. Results

3.1. Titer-dependent motor deficits are seen in mice expressing mutant ATXN3

In order to express full-length ATXN3 that includes an abnormally expanded (Q89) or normal length (Q15) polyglutamine chain in PCs of wild-type mice, we constructed AAV vector plasmids expressing human ATXN3 with an 89-polyglutamine repeat (ATXN3[Q89]) or ATXN3 with a 15-polyglutamine stretch (ATXN3[Q15]) under the control of the neuron-specific rSynI-minCMV promoter (Huda et al., 2014; Matsuzaki et al., 2014). A human influenza haemagglutinin (HA)-tag sequence was placed in frame at the 5′ end of the ATXN3 gene. In addition, the vector was designed to independently express GFP simultaneously with the ATXN3 protein by insertion of a sequence of the 2A peptide derived from porcine teschovirus-1 (P2A) (Donnelly et al., 2001) between GFP and HA-ATXN3 (Fig. 1A).

We injected AAV9 vectors expressing abnormal ATXN3[Q89] (3×10^{11} or 1×10^{11} vg) or normal ATXN3[Q15] (3×10^{11} vg) into 5-week-old wild-type mice, and assessed the influence of these expressed proteins on motor ability 3 weeks post-injection by a rotarod test (Fig. 1B). Mice that received cerebellar injection of AAV9 vectors expressing ATXN3[Q15] (3×10^{11} vg; Q15 mice) showed good rotarod performance almost identical to PBS-injected control mice, whereas mice treated with a similar titer (3×10^{11} vg) of AAV9 vectors expressing ATXN3[Q89] (Q89 mice) showed significantly poorer rotarod performance than PBS-injected control mice and Q15 mice (Fig. 1C, D; control; 197.6 ± 19.6 s, Q15; 169.4 ± 19.2 s, Q89; 99.2 ± 9.6 s, Q89 (lower titer: 1×10^{11} vg); 133.3 ± 17.6 s, control vs Q89; $P < 0.01$, Q15 vs Q89; $P < 0.05$. $P > 0.05$ in other pairs). Thus, in the remaining experiments we used the higher titer (3×10^{11} vg) of AAV9 vectors to determine the influence ATXN3[Q89] expression has on the morphology and electrophysiology of the cerebellum.

3.2. Generation of ubiquitin-positive nuclear aggregates of ATXN3[Q89] in PCs

Nuclear aggregation of a mutant protein is a pathological hallmark of polyglutamine diseases, including SCA3 (Costa Mdo and Paulson, 2012). We therefore examined whether ATXN3[Q89] that was expressed by AAV vectors also caused the formation of nuclear aggregates. Cerebellar sections from Q15 mice and Q89 mice were triple immunostained for HA tagged with ATXN3, ubiquitin, and GFP. Only subtle immunoreactivity to HA was detected throughout the cell bodies and dendrites of PCs without ubiquitin immunolabeling in Q15 mice (Fig. 1E, left panels). In contrast, a clear aggregation of HA (ATXN3[Q89]) was observed in PC nuclei of Q89 mice, which overlapped with ubiquitin immunostaining (Fig. 1E, right panels).

3.3. PC dendritic atrophy

To examine the consequence of mutant protein expression on PC morphology, PCs were visualized by infusion of biocytin into a single PC through a whole cell-clamped patch pipette, followed by the staining for biocytin with Alexa-594-conjugated streptavidin. Q15 mouse PCs showed well differentiated dendrites comparable to those of PBS-injected mice, whereas Q89 mouse PCs were significantly atrophied (Fig. 2A). The regression of Q89 mouse PC dendrites was confirmed by membrane capacitance (Cm) of PCs, which reflects the surface area of the plasma membrane (Fig. 2B, control; 580.1 ± 56.2 pF, Q15; 579.9 ± 58.6 pF, Q89; 279.2 ± 28.2 pF, control vs Q15; $P > 0.999$, control vs Q89; $P < 0.001$, Q15 vs Q89; $P < 0.001$).

3.4. Significant decrease of RORα protein in PC nuclei of Q89 mice

Studies have shown that RORα is required for the maintenance of the dendritic arborization in PCs (Chen et al., 2013; Mitsumura et al., 2011; Takeo et al., 2015). To determine whether full-length ATXN3[Q89] reduced RORα in PC nuclei similar to what was observed with the truncated ATXN3 in our previously published study of SCA3 transgenic mice (Konno et al., 2014), we examined levels of RORα by using immunohistochemistry. Sagittal sections of the cerebellum were triple-immunolabeled for GFP, RORα, and calbindin D28K (a marker for PCs) and examined by confocal laser-scanning microscopy. GFP was observed in PCs and in the molecular layer interneurons in AAV9 vector-treated mice (Fig. 3A). Robust immunoreactivity for RORα was detected in PC nuclei from PBS-treated mice and Q15 mice, in addition to a modest expression in the molecular layer interneurons (Fig. 3A, B). In contrast, RORα immunoreactivity in PC nuclei was significantly lower in Q89 mice (Fig. 3A, B, control vs Q15; $P > 0.999$, control vs Q89; $P < 0.001$, Q15 vs Q89; $P < 0.001$). In order to determine whether the lower levels of RORα were due to the reduced production or enhanced degradation, we used quantitative RT-PCR to examine the levels of RORα mRNA in the cerebellum. The levels of RORα mRNAs in Q89 mouse cerebella were comparable to that seen in the PBS-injected mice and in the Q15 mice (Fig. 3C), suggesting that reduction in RORα protein in Q89 mouse PCs were likely due to enhanced protein degradation.

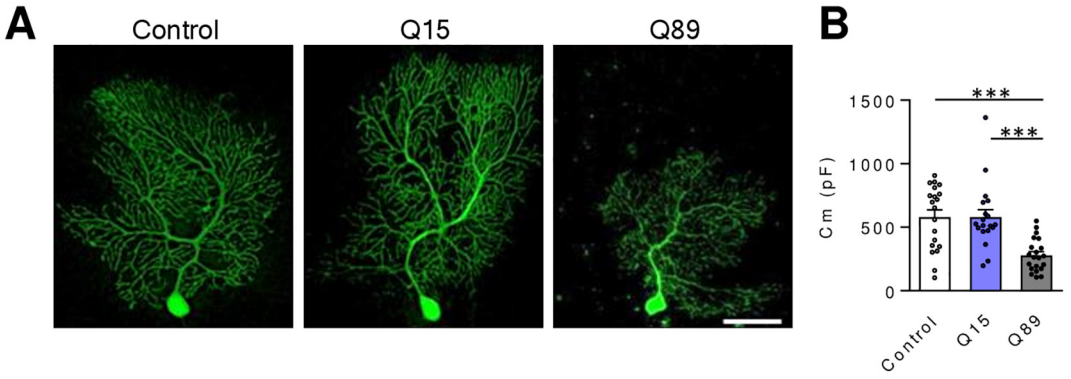

Fig. 2. Degeneration of PC dendrites in mice expressing ATXN3[Q89].
(A) Representative PCs from mice that had received an injection of PBS (control) and those expressing ATXN3[Q15] (Q15) or ATXN3[Q89] (Q89). PC morphology was visualized by infusion of biocytin through a whole cell-clamped patch electrode, followed by detection of biocytin in PCs using Alexa-594 conjugated-streptavidin. Scale bar indicates 50 μm. (B) The graph shows membrane capacitance (Cm) of PCs from control mice, Q15 mice and Q89 mice (control: 20 PCs from 7 mice, Q15: 19 PCs from 5 mice, Q89: 21 PCs from 7 mice). Asterisks indicate statistically significant differences, as determined by one-way ANOVA followed by Bonferroni's post hoc test. ***P < 0.001. PBS; phosphate-buffered saline, PC; Purkinje cell.

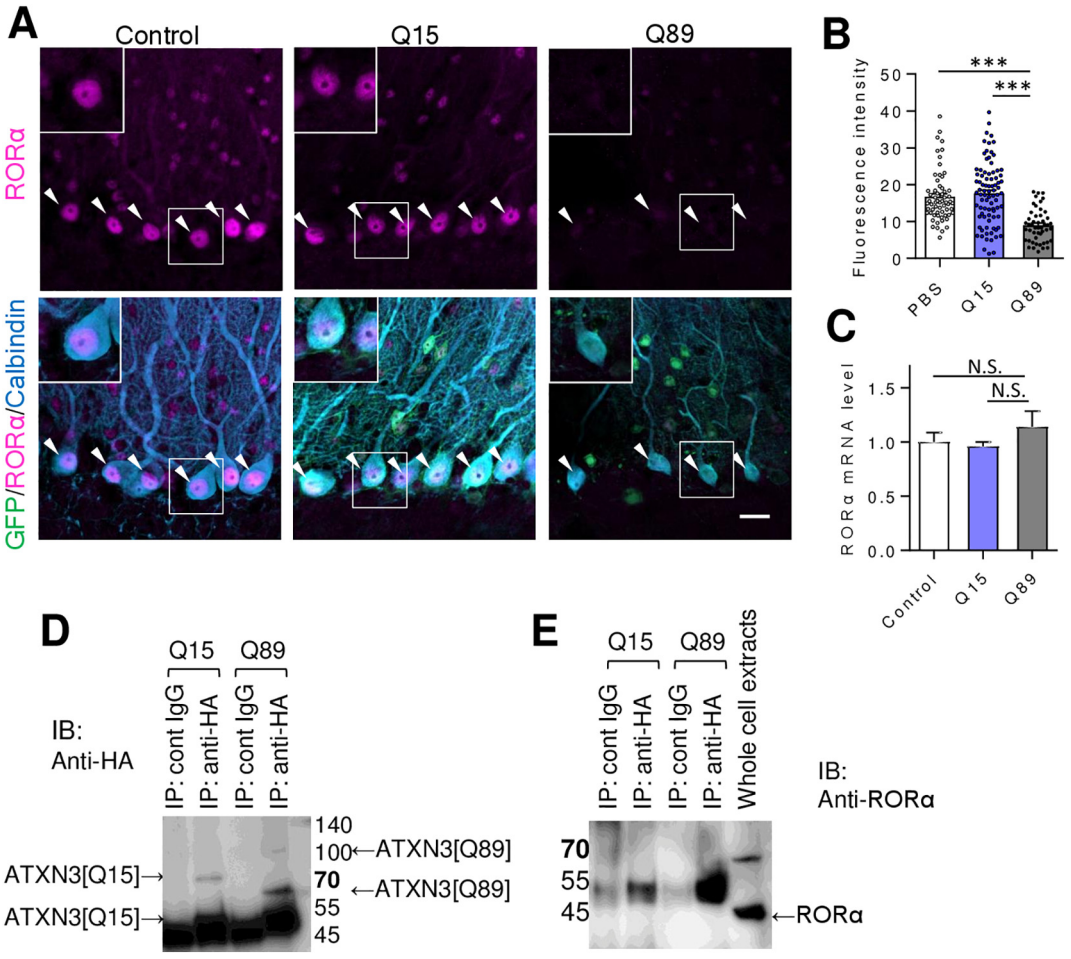

Fig. 3. Significant reduction in RORα protein in PC nuclei.
(A) Immunohistochemistry of the cerebellar cortex from mice that had received an injection of PBS (control) and those expressing ATXN3[Q15] (Q15) or ATXN3[Q89] (Q89). Sagittal sections triple immunolabeled for GFP (green), RORα (magenta), and calbindin (light blue) were examined by a confocal microscope. Scale bar indicates 20 μm. (B) Quantification of RORα immunoreactivity in PC nuclei (control: 63 PCs from 5 mice, Q15: 84 PCs from 6 mice, Q89: 49 PCs from 5 mice). (C) mRNA levels of RORα in the cerebellum was determined by quantitative RT-PCR (3 mice in each group). (D, E) Failure of co-immunoprecipitation of RORα with ATXN3. HA-tagged ATXN3[Q15] or ATXN3[Q89] was immunoprecipitated with anti-HA antibody or control IgG. Immunoblotting with anti-HA antibody (IB: Anti-HA) revealed presence of 2 sizes of ATXN3[Q15] or ATXN3[Q89] (D). Upper thinner bands correspond to undigested ATXN3-GFP. Immunoblotting with anti-RORα antibody (IB: Anti-RORα) showed no co-immunoprecipitation of RORα (E), although it was clearly detected in the whole cerebellar extracts. Asterisks indicate statistically significant differences as determined by one-way ANOVA followed by Bonferroni's post hoc test. ***P < 0.001, N.S., not significant. PBS; phosphate-buffered saline, PC; Purkinje cell, RORα; retinoid-related orphan receptor α, RT-PCR; quantitative reverse transcription polymerase chain reaction.

A previous study showed that RORα formed a transcriptional complex with normal ATXN1, but not with ATXN1 carrying abnormally long polyglutamine tract (Serra et al., 2006), and failure of the complex formation resulted in RORα degradation. These findings suggested that, similar to ATXN1, normal ATXN3 (ATXN3[Q15]), but not abnormal ATXN3[Q89], may form a complex with RORα, which could explain for the reduction in RORα in ATXN3[Q89]-expressing PCs. To validate this idea, we performed an immunoprecipitation experiment using the anti-HA antibody. Both (HA-tagged) ATXN3[Q15] and (HA-tagged) ATXN3[Q89] were reasonably immunoprecipitated with anti-HA antibody in Q15 mouse and Q89 mouse, respectively (Fig. 3D). However, immunoblotting with anti-RORα antibody failed to detect RORα in the precipitates (Fig. 3E). These results suggested that, unlike ATXN1, ATXN3 did not bind to RORα and thus, decrease in RORα protein in Q89 mouse PCs may be a consequence of non-specific degradation in degenerating PCs.

3.5. Decrease in multiple proteins in Q89 mouse PCs

We assessed various PC-specific protein levels in ATXN3[Q89]-expressing PCs by Western blotting. Because it is difficult to obtain identical transduction by direct viral injection, the tissue samples may contain different amounts of untransduced tissues, which could mask a significant difference, even if ATXN3[Q89] alters expression levels of some proteins in PCs. Thus, we used intravenous injection of AAV-PHP·B, which showed a high permeability to the blood–brain barrier and caused a global and efficient transduction of the brain (Supplementary Fig. 1A) (Deverman et al., 2016). The systemic administration of AAV-PHP·B expressing ATXN3[Q89] leads to similar phenotypes as those that received a direct cerebellar injection of AAV9 vectors, in terms of poor rotarod performance, ubiquitinated aggregate formation in the PC nuclei, and reduced immunoreactivity to RORα (Supplementary Fig. 1B–E). Western blot analysis revealed that the amounts of the ionotropic glutamate receptor delta 2 subunit (GluD2), mGluR1, and inositol 1,4,5-triphosphate receptor type 1 (IP_3R1) in ATXN3[Q89]-expressing PCs were significantly lower than those in ATXN3[Q15]-expressing PCs (Fig. 4A–D), while there were no significant differences in the amounts of transient receptor potential cation channel type 3 (TRPC3) and GFP between two mouse groups (Fig. 4E, F). Because GluD2 is expressed specifically in PCs, but not under the control of RORα-mediated transcription, the reduction in GluD2 seems to be a consequence of a non-specific downregulation of protein expression accompanying PC degeneration. By contrast, expression of mGluR1 and IP_3R1 is associated with RORα-mediated transcription (Lin et al., 2000; Serra et al., 2006), and reduced levels of mGluR1 and IP_3R1 in ATXN3[Q89]-expressing PCs could be a result of RORα degradation, in addition to a global alteration in protein expression accompanying PC degeneration.

3.6. mGluR1 signaling defects in Q89 mice

Since the amounts of mGluR1 and IP_3R1 were decreased in Q89 mouse PCs, we evaluated mGluR1 signaling in PC by measuring the amplitude of slow EPSCs and long-term depression (LTD) at the synapses of parallel fibers (PF) onto the PCs. TRPC3-mediated slow EPSCs (Hartmann et al., 2008) were elicited in PC following repetitive electrical stimulation of PFs (5 pulses at 100 Hz) with increasing stimulus intensities. To eliminate AMPA receptor-mediated fast EPSCs, 20 μM NBQX, an AMPA receptor antagonist, was included in the extracellular solution. It is well established that slow EPSCs are triggered by mGluR1 activation, since CPCCOEt, a mGluR1 antagonist, completely blocks the corresponding current (Canepari et al., 2001). In PBS-injected mouse PCs, slow EPSCs became larger as the stimulus intensity increased, and reached over 300 pA at a stimulus level of 100 μA (Fig. 5A, B). A similar increase in slow EPSC amplitude was observed in Q15 mouse PCs. There is no statistically significant difference in the amplitude of the slow EPSCs between PBS-injected mice and Q15 mice. In contrast, the amplitude in Q89 mouse PCs remained only ~70 pA even at a 100 μA stimulus (Fig. 5A, B, control; 342.4 ± 69.4 pA, Q15; 267.8 ± 44.9 pA, Q89; 72.3 ± 20.2 pF, control vs Q15; $P > 0.5$, control vs Q89; $P < 0.01$, Q15 vs Q89; $P < 0.05$), indicating a marked impairment in the generation of slow EPSC in PCs that express ATXN3[Q89].

mGluR1 activation is indispensable for LTD expression at synapses between PFs and PCs (Aiba et al., 1994). mGluR1 activates protein

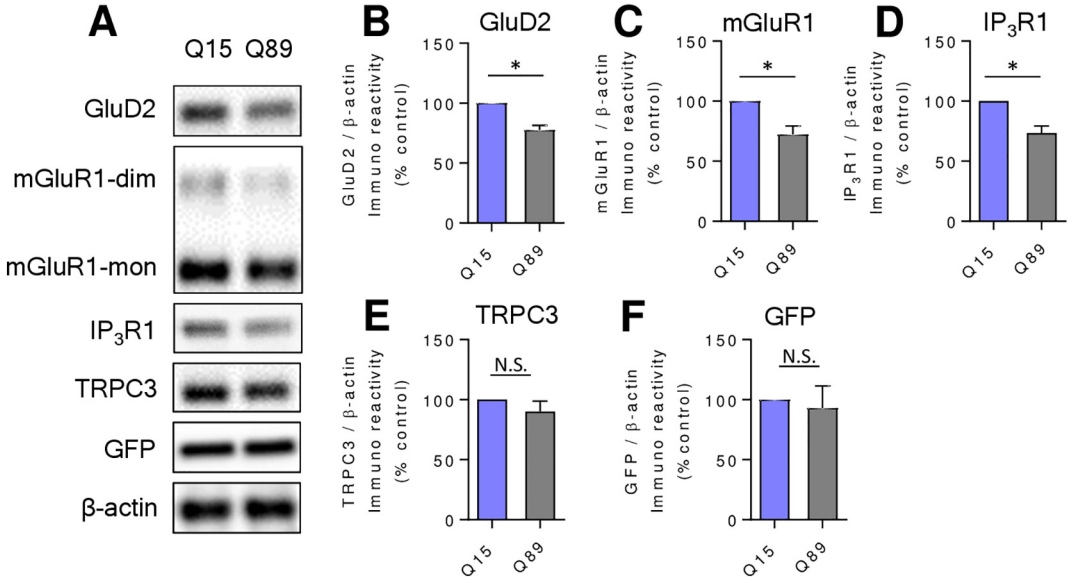

Fig. 4. Alteration in PC-specific protein levels by ATXN3[Q89] expression.
Western blot analysis of protein extracts from cerebella virally expressing mutant ATXN3. Mice received intravenous injection of AAV-PHP.B expressing ATXN3[Q15] or ATXN3[Q89] together with GFP under the control of CBh promoter (See supplementary Fig. 1A). (A) Cerebellar vermises were subjected to western blotting 3 weeks after the injection with antibodies as depicted. (B-F) Quantitative analysis of band intensities immunoreactive to GluD2 (B), mGluR1 (C), IP3R1 (D), TRPC3 (E) and GFP (F). Each band intensity was normalized by that of β-actin. Asterisks indicate statistically significant differences as determined by one sample t-test. *$P < 0.05$. N.S., not significant. GluD2; ionotropic glutamate receptor delta 2 subunit, IP3R1; inositol 1,4,5-triphosphate receptor type 1, mGluR1-dim; mGluR1 dimer, mGluR1-mon; mGluR1-monomer, TRPC3; transient receptor potential cation channel type 3.

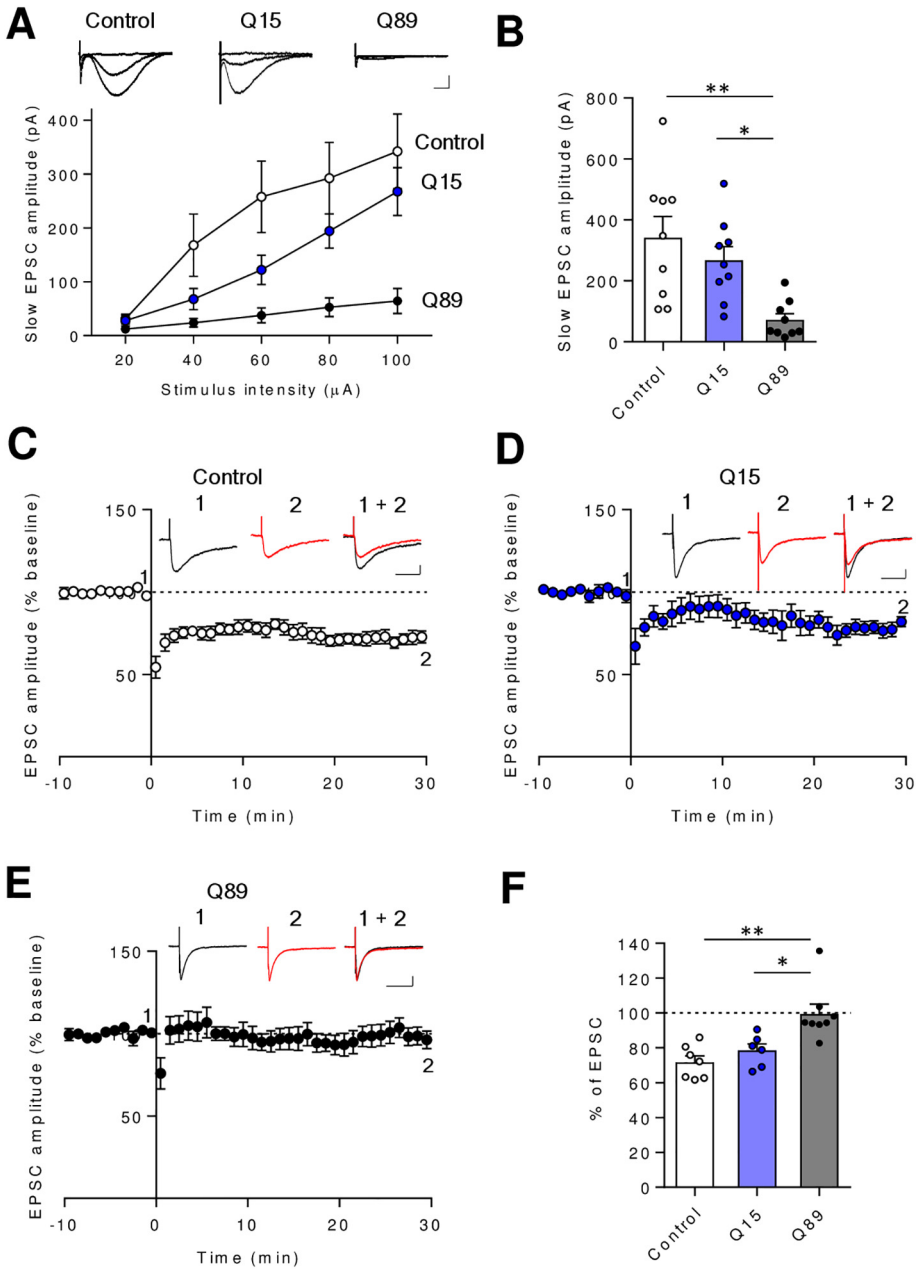

Fig. 5. Expression of ATXN3[Q89] disrupts mGluR1 signaling in PCs. (A) Significant attenuation of mGluR1-mediated slow EPSCs in PCs expressing ATXN3[Q89]. Slow EPSCs were elicited from PCs in response to repetitive PF stimulation (5 times at 100 Hz) at increasing stimulus intensities. Representative traces of slow EPSCs at 20 μA, 60 μA, and 100 μA stimulus intensities are presented above the graph. Scale bar indicates 100 pA, 500 ms. (B) Graph showing amplitudes of slow EPSCs evoked at 100 μA stimulation (control: 9 PCs from 4 mice, Q15: 9 PCs from 4 mice, Q89: 9 PCs from 6 mice). (C-E) Deficient cerebellar LTD in PCs expressing ATXN3[Q89]. Conjunctive stimulation of PF (1 Hz, 30 s) with depolarization of PC was applied at time 0. The averaged amplitudes of PF-EPSCs over 1 min were normalized to the baseline value, which was the average of the 10-min responses (60 traces) that occurred just before conjunctive stimulation. LTD was reliably induced in PCs from mice treated with PBS (control) (C) and those from mice expressing ATXN3[Q15] (D). In contrast, LTD expression was disrupted in PCs from mice expressing ATXN3[Q89] (E). Representative traces before (1), and 30 min after (2), the conjunctive stimulation is shown in black and red lines respectively, as well as the superimposed images (1 + 2). Scale bar 50 pA, 50 ms. (F) Summarized graph showing depression ratios, which were calculated by dividing the averaged EPSC amplitude values from 25 to 30 min post-induction by those from −10 to 0 min (control: 7 PCs from 6 mice, Q15: 6 PCs from 4 mice, Q89: 8 PCs from 6 mice). Asterisks indicate statistically significant differences as determined by one-way ANOVA followed by Bonferroni's post hoc test. *P < 0.05, **P < 0.01. EPSC; excitatory postsynaptic current, LTD; long-term depression, PC; Purkinje cell, PF; parallel fiber.

kinase C (PKC), which in turn phosphorylates the GluA2 subunit of postsynaptic AMPA receptors, leading to endocytosis of the AMPA receptors (Chung et al., 2003; Hirai 2001; Matsuda et al., 2000). LTD was induced by PF stimulation (30 times at 1 Hz) in conjunction with PC depolarization (Hirai et al., 2003). LTD was reliably induced in PBS-injected PCs and Q15 mouse PCs, whereas LTD expression was clearly disrupted in Q89 mouse PCs (Fig. 5C–F, control; 71.7 ± 3.7%, Q15; 78.5 ± 3.8%, Q89; 99.5 ± 5.6%). These results suggest that mGluR1 signaling is impaired selectively in Q89 mouse PCs.

If mGluR1 signaling defects underlie the failure of LTD expression in Q89 PCs, the phenotype may be ameliorated by enhancement of mGluR1 function. To validate this possibility, we injected Ro0711401, a mGluR1 PAM, subcutaneously into Q89 mice 3 weeks after injection of AAV9 vector expressing ATXN3[Q89]. The effect of the injections was assessed 30 min post-injection by rotarod (Fig. 6A). The Q89 mice treated with Ro0711401 showed a significantly better performance than non-treated Q89 mice (Fig. 6B, C, Q89; 76.0 ± 11.6 s, Q89 + Ro0711401; 114.8 ± 10.5 s, P < 0.05), supporting our idea that the mGluR1 signaling defects contribute, at least partially, to the motor deficit seen in Q89 mice.

3.7. Administration of RORα/γ agonist suppresses abnormal phenotypes in Q89 mice

To verify whether the decrease in RORα levels in PCs plays a key role in the motor deficit seen in Q89 mice, RORα function in Q89 mouse PCs was reinforced by SR1078, an RORα/γ agonist (Wang et al., 2016; 2010). SR1078 (10 mg/kg) was intraperitoneally injected into Q89 mice 1 week after the AAV9 vector injection, and the motor ability was assessed 2 weeks after the SR1078 treatment (Fig. 7A). Q89 mice that received injection of SR1078 showed significantly better rotarod performance than control Q89 mice that did not receive SR1078 injection (Fig. 7B, C, Q89; 79.4 ± 11.3 s, Q89 + SR1078; 122.9 ± 17.1 s, P < 0.05).

We next examined the influence of SR1078 injection on dendritic morphology of Q89 mouse PCs. PCs from SR1078-treated Q89 mice

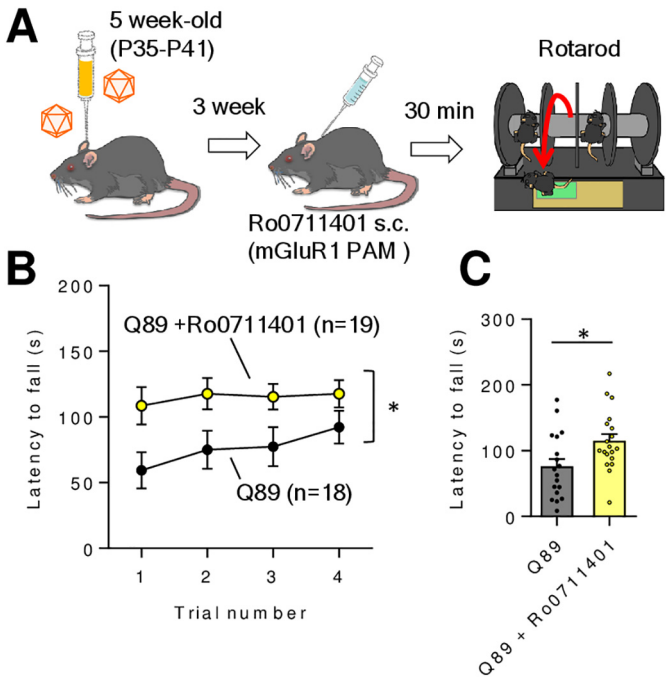

Fig. 6. Significantly better rotarod performance in Q89 mice treated with mGluR1 PAM than in non-treated Q89 mice. (A) Schematic depicting the experimental paradigm. Ro0711401, a mGluR1 PAM, was injected subcutaneously 3 weeks after injection of AAV9 vector expressing ATXN3[Q89]. The effect of Ro0711401 on the motor function was examined by rotarod 30 min after the injection. (B) Results of the rotarod. Each mouse was subjected to 4 trials. (C) Summarized graph showing the average of the 4 trials. Asterisks indicate statistically significant differences as determined by unpaired t-test or by repeated measured ANOVA. *P < 0.05. AAV9; adeno-associated virus serotype 9, PAM; positive allosteric modulator.

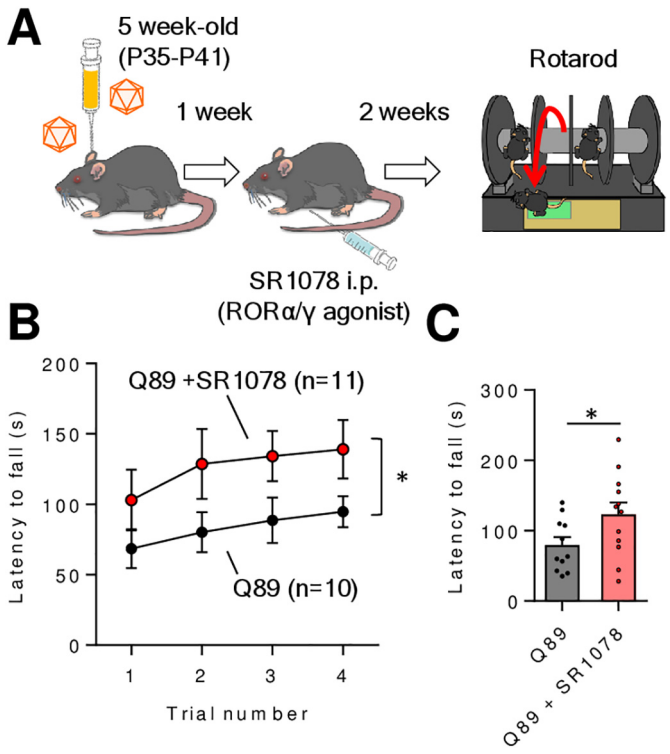

Fig. 7. Significantly improved rotarod performance in Q89 mice treated with a RORα/γ agonist compared to non-treated Q89 mice.
(A) Schematic depicting the experimental paradigm. SR1078, a RORα/γ agonist, was injected intraperitoneally 1 week after injection of AAV9 vectors expressing ATXN3[Q89]. The effect of SR1078 on the motor function was examined 2 weeks after the injection by rotarod. (B) Results of the rotarod. Each mouse was subjected to 4 trials. (C) Summarized graph showing the average of the 4 trials, indicating significantly better performance in Q89 mice treated with SR1078. Asterisks indicate statistically significant differences as determined by unpaired t-test or by repeated measured ANOVA. *P < 0.05. RORα/γ; retinoid-related orphan receptor α/γ.

showed dendrites with larger ramifications comparable to those from PBS-injected control mice, and more extensive than those from non-treated Q89 mice (Fig. 8A, B). We then evaluated the effect of SR1078 injection on mGluR1 signaling. Slow EPSCs were evoked by repetitive PF stimulation with increasing electrical stimulation, as described above. The amplitude of the slow EPSC in PCs from SR1078-treated Q89 mice was ~280 pA at a 100 μA stimulus, which was markedly larger than those of non-treated Q89 mice (~70 pA) (Fig. 8C, D, Q89 + SR1078; 280.3 ± 48.2 pA, P < 0.001). Moreover, robust LTD at synapses between PF and PC was induced in PCs from SR1078-treated Q89 mice (Fig. 8E, F, Q89 + SR1078; 73.9 ± 4.7%, P < 0.01). These results suggest that SR1078 effectively inhibits dendritic degeneration and mGluR1 signaling defects in Q89 mouse PCs.

4. Discussion

In this report, full-length ATXN3 comprising an abnormally expanded (Q89) or normal length (Q15) of polyglutamine was expressed virally in the cerebella of wild-type mice. Although expression levels of both transgenes seemed almost identical, as judged from levels of GFP, mice that expressed abnormal ATXN3[Q89], but not normal ATXN3[Q15], experienced a degeneration of the dendritic tree, in parallel with the downregulation of multiple proteins including RORα and mGluR1 signaling molecules, in PCs, resulting in motor deficit. As reported previously (Huda et al., 2014), direct cerebellar injection of AAV9 vectors restricts the transgene expression primarily to the cerebellum with modest expression in the pontine nuclei, and an almost complete absence of transduced cells in other brain regions including the cerebrum and the spinal cord. Moreover, use of the neuron-specific SynI-minCMV promoter limits the expression to the CNS. Thus, motor deficits in mice were likely due to abnormal ATXN3[Q89]-induced impairment of the cerebellum. Notably, the morphological, functional, and behavioral phenotypes were largely reversed by a single intraperitoneal injection of SR1078, an RORα/γ agonist. Subcutaneous injection of Ro0711401, an mGluR1 PAM, also mitigated motor impairment caused by mutant ATXN3 expression, suggesting that downregulation of RORα and accompanying attenuation of mGluR1 signaling play pivotal roles in aberrant phenotypes in Q89 mice.

Our immunoprecipitation experiment showed that, unlike ATXN1 (Serra et al., 2006), ATXN3 did not bind to RORα. Thus, the mechanism underlying the downregulation of RORα in SCA3 is different from that of SCA1, and may be due to non-specific protein degradation, secondary to PC degeneration. On the other hand, reduced levels of RORα were shown to cause morphological and functional defects in PCs. For example, classical ataxic *staggerer* mice that lack functional RORα display a marked maldevelopment of PC dendrites and severe mGluR1 signaling defects (Hamilton et al., 1996; Mitsumura et al., 2011; Sidman et al., 1962). The deletion of RORα in adult $Rora^{fl/fl}$ PCs by lentiviral vector-mediated expression of Cre recombinase (Chen et al., 2013) or tamoxifen-induced knockout of RORα from over 3-week-old PCs by CRISPR/Cas9 (Takeo et al., 2015), resulted in atrophy of PC dendrites. Moreover, our preliminary data showed that RORα knockdown in mature wild-type PCs caused PC dendritic atrophy and progressive motor impairment. These data suggest that RORα is indispensable for the maintenance of dendrite arborization and mGluR1 signaling in PCs.

RORα binds to promotor elements of numerous genes and controls expression of > 6000 genes in the brain (Sarachana and Hu 2013),

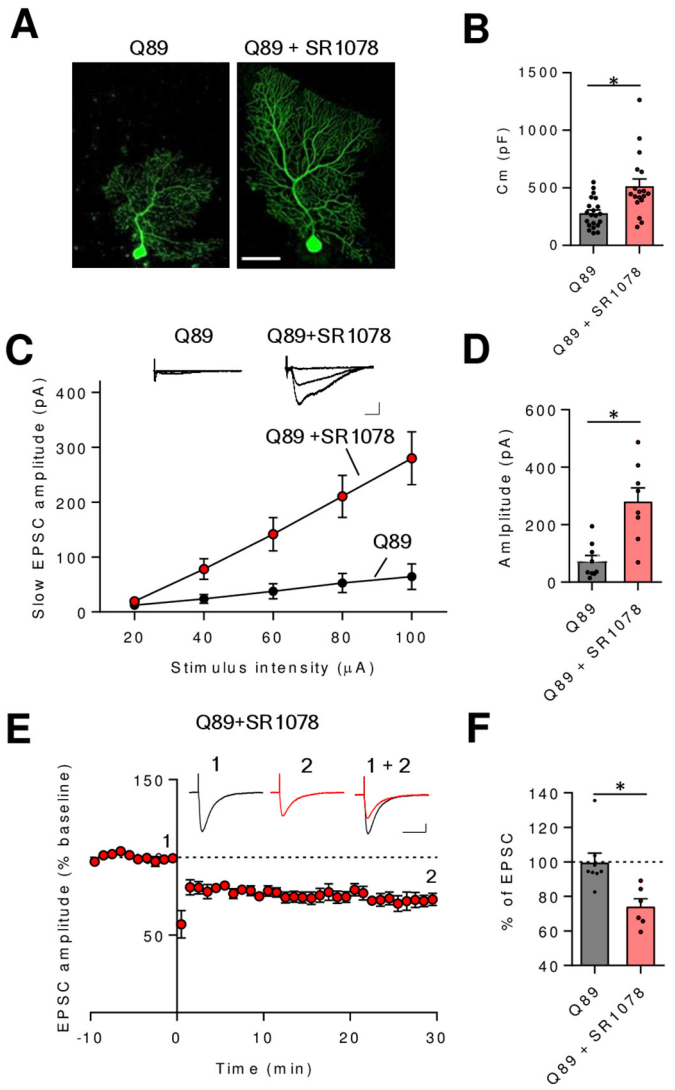

Fig. 8. Pharmacological upregulation of RORα in Q89 mice prevents the emergence of aberrant phenotypes. Q89 mice received an intraperitoneal injection of SR1078, an RORα/γ agonist, 3 weeks after injection of AAV9 vectors expressing ATXN3[Q89]. (A) Representative biocytin-infused PCs from Q89 mice without or with SR1078 injection. PCs were visualized by Alexa-594 conjugated-streptavidin. Scale bar indicates 50 μm. (B) Graph showing membrane capacitance (Cm) of PCs from Q89 mice without or with SR1078 injection (Q89: 21 PCs from 7 mice, Q89 + SR1078: 18 PCs from 5 mice), indicating a significant suppression of PC dendrite degeneration by SR1078. (C) Efficient generation of slow EPSCs in PCs from Q89 mice treated with SR1078. PCs from Q89 mice treated with SR1078 produced larger amplitude of slow EPSC than that from non-injected Q89 mice. Representative traces of slow EPSCs at 20 μA, 60 μA, and 100 μA stimulus intensities are presented above the graph. Scale bar indicates 100 pA, 500 ms. (D) Graph showing amplitudes of slow EPSCs evoked at 100 μA stimulation (Q89: 9 PCs from 6 mice, Q89 + SR1078: 18 PCs from 5 mice). (E) Expression of robust LTD in PCs from Q89 mice treated with SR1078. Representative traces before (1), and 30 min after (2), the conjunctive stimulation are shown in black and red lines respectively, as well as the superimposed images (1 + 2). Scale bar indicates 50 pA, 50 ms. (F) Summarized graph showing depression ratios, which were calculated by dividing the averaged EPSC amplitude values from 25 to 30 min by those from −10 to 0 min (Q89: 8 PCs from 6 mice, Q89 + SR1078: 8 PCs from 5 mice). The data of control Q89 in (A-D and F), which were same as shown in other figures, were presented for comparison. Asterisks indicate statistically significant differences as determined by one-way ANOVA followed by Bonferroni's post hoc test. *P < 0.05. EPSC; excitatory postsynaptic current, LTD; long-term depression, PC; Purkinje cell, RORα/γ; retinoid-related orphan receptor α/γ.

including mGluR1 signaling molecules (Lin et al., 2000; Serra et al., 2006) and the PCP2/L7 protein (Nitta et al., 2017). A recent study identified RORα gene (*RORA*) mutations in 16 human individuals from 13 families (Guissart et al., 2018). These individuals showed variable neurodevelopmental defects, which were primarily characterized by autistic features and cerebellar phenotypes. Notably, haploinsufficiency of the *RORA* gene is closely associated with cerebellar hypoplasia and cerebellar ataxia in individuals with a mutant *RORA* (Guissart et al., 2018). These findings of pathologies in human individuals carrying *RORA* mutations, together with our present results, strongly support the notion that RORα deficiency in PCs could play a crucial role in the progressive cerebellar atrophy and cerebellar ataxia also seen in SCA3 patients.

Recent studies revealed mGluR1 signaling defects in other types of SCAs (Hirai and Kano 2018) such as SCA15/SCA16 and SCA41. SCA15/SCA16 are caused by deletion/missense mutation in *ITPR1* (Hisatsune and Mikoshiba 2017), while SCA41 is due to a missense mutation in *TRPC3* (SCA41) (Fogel et al., 2015). Thus, SCA15/SCA16 and SCA41 also cause aberrant mGluR1 signaling, resulting in cerebellar ataxia. Since augmentation of RORα function by SR1078 prevented degeneration of PC dendrites and a deterioration of mGluR1 signaling in mice expressing abnormal ATXN3[Q89], RORα could be a promising therapeutic target for SCA3 and potentially other types of SCAs that compromise mGluR1 signaling pathway in PCs.

Pharmacological augmentation of mGluR1 function by Ro0711401 (Notartomaso et al., 2013) or baclofen (Shuvaev et al., 2017) could be a reasonable approach to mitigate SCA3 pathology. However, RORα enhancement is thought to be superior in terms of the benefit toward PC dendrite degeneration, since a mGluR1 defect does not likely contribute to PC dendrite degeneration (Aiba et al., 1994). In contrast, RORα plays pivotal roles in both the development/maintenance of dendritic trees and in mGluR1 signaling in PCs (Chen et al., 2013; Hirai and Kano 2018; Takeo et al., 2015).

5. Conclusions

Expression of abnormal ATXN3[Q89] triggered PC degeneration in addition to (probably global) downregulation of transcriptional and signaling proteins including RORα and mGluR1, resulting in motor deficit. Augmentation of RORα function by SR1078 significantly prevented dendritic degeneration and mGluR1 signaling defects in PCs as well as motor deficit. Thus, we propose that the mutant-ATXN3-triggered RORα deficiency plays a key role in the molecular basis of the SCA3 pathology. The present findings suggest that pharmacological augmentation of RORα function could be promising as a therapeutic intervention against SCA3.

Supplementary data to this article can be found online at https://doi.org/10.1016/j.nbd.2018.10.014.

Author contributions

H.H. and M.W. designed the experiments; M.W., C.H., A.K., Y.F., Y.M. and T.I. performed the research; M.W. analyzed the data; M.W. and H.H. wrote the paper.

Declarations of interest

None.

Funding

This work was supported by JSPS KAKENHI (Grant Numbers 15H04254, 18H02521, 15K18330, 17K14929). Grants were obtained from the program for Brain Mapping by Integrated Neurotechnologies for Disease Studies (Brain/MINDS), Japan Agency for Medical Research and Development (AMED); Research on Measures for Intractable

Diseases (Ataxic Diseases and Neurodegenerative Diseases), Ministry of Health, Labor and Welfare, and the Gunma University Initiative for Advanced Research (GIAR).

Acknowledgements

The authors thank Asako Ohnishi for the AAV9 vector production.

References

Aiba, A., Kano, M., Chen, C., Stanton, M.E., Fox, G.D., Herrup, K., Zwingman, T.A., Tonegawa, S., 1994. Deficient cerebellar long-term depression and impaired motor learning in mGluR1 mutant mice. Cell 79, 377–388.

Boukhtouche, F., Doulazmi, M., Frederic, F., Dusart, I., Brugg, B., Mariani, J., 2006. RORalpha, a pivotal nuclear receptor for Purkinje neuron survival and differentiation: from development to ageing. Cerebellum 5, 97–104.

Canepari, M., Papageorgiou, G., Corrie, J.E., Watkins, C., Ogden, D., 2001. The conductance underlying the parallel fibre slow EPSP in rat cerebellar Purkinje neurones studied with photolytic release of L-glutamate. J. Physiol. 533, 765–772.

Chen, X.R., Heck, N., Lohof, A.M., Rochefort, C., Morel, M.P., Wehrle, R., Doulazmi, M., Marty, S., Cannaya, V., Avci, H.X., Mariani, J., Rondi-Reig, L., Vodjdani, G., Sherrard, R.M., Sotelo, C., Dusart, I., 2013. Mature Purkinje cells require the retinoic acid-related orphan receptor-alpha (RORalpha) to maintain climbing fiber mono-innervation and other adult characteristics. J. Neurosci. 33, 9546–9562.

Chung, H.J., Steinberg, J.P., Huganir, R.L., Linden, D.J., 2003. Requirement of AMPA receptor GluR2 phosphorylation for cerebellar long-term depression. Science 300, 1751–1755.

Costa Mdo, C., Paulson, H.L., 2012. Toward understanding Machado-Joseph disease. Prog. Neurobiol. 97, 239–257.

Deverman, B.E., Pravdo, P.L., Simpson, B.P., Kumar, S.R., Chan, K.Y., Banerjee, A., Wu, W.L., Yang, B., Huber, N., Pasca, S.P., Gradinaru, V., 2016. Cre-dependent selection yields AAV variants for widespread gene transfer to the adult brain. Nat. Biotechnol. 34, 204–209.

Donnelly, M.L., Luke, G., Mehrotra, A., Li, X., Hughes, L.E., Gani, D., Ryan, M.D., 2001. Analysis of the aphthovirus 2A/2B polyprotein 'cleavage' mechanism indicates not a proteolytic reaction, but a novel translational effect: a putative ribosomal 'skip. J. Gen. Virol. 82, 1013–1025.

Fogel, B.L., Hanson, S.M., Becker, E.B., 2015. Do mutations in the murine ataxia gene TRPC3 cause cerebellar ataxia in humans? Mov. Disord. 30, 284–286.

Globas, C., du Montcel, S.T., Baliko, L., Boesch, S., Depondt, C., Didonato, S., Durr, A., Filla, A., Klockgether, T., Mariotti, C., Melegh, B., Rakowicz, M., Ribai, P., Rola, R., Schmitz-Hubsch, T., Szymanski, S., Timmann, D., Van de Warrenburg, B.P., Bauer, P., Schols, L., 2008. Early symptoms in spinocerebellar ataxia type 1, 2, 3, and 6. Mov. Disord. 23, 2232–2238.

Gray, S.J., Foti, S.B., Schwartz, J.W., Bachaboina, L., Taylor-Blake, B., Coleman, J., Ehlers, M.D., Zylka, M.J., McCown, T.J., Samulski, R.J., 2011. Optimizing promoters for recombinant adeno-associated virus-mediated gene expression in the peripheral and central nervous system using self-complementary vectors. Hum. Gene Ther. 22, 1143–11453.

Guissart, C., Latypova, X., Rollier, P., Khan, T.N., Stamberger, H., McWalter, K., Cho, M.T., Kjaergaard, S., Weckhuysen, S., Lesca, G., Besnard, T., Ounap, K., Schema, L., Chiocchetti, A.G., McDonald, M., de Bellescize, J., Vincent, M., Van Esch, H., Sattler, S., Forghani, I., Thiffault, I., Freitag, C.M., Barbouth, D.S., Cadieux-Dion, M., Willaert, R., Guillen Sacoto, M.J., Safina, N.P., Dubourg, C., Grote, L., Carre, W., Saunders, C., Pajusalu, S., Farrow, E., Boland, A., Karlowicz, D.H., Deleuze, J.F., Wojcik, M.H., Pressman, R., Isidor, B., Vogels, A., Van Paesschen, W., Al-Gazali, L., Al Shamsi, A.M., Claustres, M., Pujol, A., Sanders, S.J., Rivier, F., Leboucq, N., Cogne, B., Sasorith, S., Sanlaville, D., Retterer, K., Odent, S., Katsanis, N., Bezieau, S., Koenig, M., Davis, E.E., Pasquier, L., Kury, S., 2018. Dual molecular effects of dominant RORA mutations cause two variants of syndromic intellectual disability with either autism or cerebellar ataxia. Am. J. Hum. Genet. 102, 744–759.

Hamilton, B.A., Frankel, W.N., Kerrebrock, A.W., Hawkins, T.L., Fitzhugh, W., Kusumi, K., Russell, L.B., Mueller, K.L., van Berkel, V., Birren, B.W., Kruglyak, L., Lander, E.S., 1996. Disruption of the nuclear hormone receptor RORalpha in staggerer mice. Nature 379, 736–739.

Hartmann, J., Dragicevic, E., Adelsberger, H., Henning, H.A., Sumser, M., Abramowitz, J., Blum, R., Dietrich, A., Freichel, M., Flockerzi, V., Birnbaumer, L., Konnerth, A., 2008. TRPC3 channels are required for synaptic transmission and motor coordination. Neuron 59, 392–398.

Hirai, H., 2001. Modification of AMPA receptor clustering regulates cerebellar synaptic plasticity. Neurosci. Res. 39, 261–267.

Hirai, H., Kano, M., 2018. Type 1 metabotropic glutamate receptor and its signaling molecules as therapeutic targets for the treatment of cerebellar disorders. Curr. Opin. Pharmacol. 38, 51–58.

Hirai, H., Launey, T., Mikawa, S., Torashima, T., Yanagihara, D., Kasaura, T., Miyamoto, A., Yuzaki, M., 2003. New role of delta2-glutamate receptors in AMPA receptor trafficking and cerebellar function. Nat. Neurosci. 6, 869–876.

Hisatsune, C., Mikoshiba, K., 2017. IP3 receptor mutations and brain diseases in human and rodents. J. Neurochem. 141, 790–807.

Huda, F., Konno, A., Matsuzaki, Y., Goenawan, H., Miyake, K., Shimada, T., Hirai, H., 2014. Distinct transduction profiles in the CNS via three injection routes of AAV9 and the application to generation of a neurodegenerative mouse model. Mol. Ther. Methods Clin. Dev. 1, 14032.

Iizuka, A., Matsuzaki, Y., Konno, A., Hirai, H., 2016. Plasticity of the developmentally arrested staggerer cerebellum in response to exogenous RORalpha. Brain Struct. Funct. 221, 2879–2889.

Ikeda, H., Yamaguchi, M., Sugai, S., Aze, Y., Narumiya, S., Kakizuka, A., 1996. Expanded polyglutamine in the Machado-Joseph disease protein induces cell death in vitro and in vivo. Nat. Genet. 13, 196–202.

Kawaguchi, Y., Okamoto, T., Taniwaki, M., Aizawa, M., Inoue, M., Katayama, S., Kawakami, H., Nakamura, S., Nishimura, M., Akiguchi, I., et al., 1994. CAG expansions in a novel gene for Machado-Joseph disease at chromosome 14q32.1. Nat. Genet. 8, 221–228.

Konno, A., Shuvaev, A.N., Miyake, N., Miyake, K., Iizuka, A., Matsuura, S., Huda, F., Nakamura, K., Yanagi, S., Shimada, T., Hirai, H., 2014. Mutant ataxin-3 with an abnormally expanded polyglutamine chain disrupts dendritic development and metabotropic glutamate receptor signaling in mouse cerebellar Purkinje cells. Cerebellum 13, 29–41.

Laccone, F., Maiwald, R., Bingemann, S., 1999. A fast polymerase chain reaction-mediated strategy for introducing repeat expansions into CAG-repeat containing genes. Hum. Mutat. 13, 497–502.

Li, X., Liu, H., Fischhaber, P.L., Tang, T.S., 2015. Toward therapeutic targets for SCA3: insight into the role of Machado-Joseph disease protein ataxin-3 in misfolded proteins clearance. Prog. Neurobiol. 132, 34–58.

Libbey, J.E., Hanak, T.J., Doty, D.J., Wilcox, K.S., Fujinami, R.S., 2016. NBQX, a highly selective competitive antagonist of AMPA and KA ionotropic glutamate receptors, increases seizures and mortality following picornavirus infection. Exp. Neurol. 280, 89–96.

Lin, X., Antalffy, B., Kang, D., Orr, H.T., Zoghbi, H.Y., 2000. Polyglutamine expansion down-regulates specific neuronal genes before pathologic changes in SCA1. Nat. Neurosci. 3, 157–163.

Matsuda, S., Launey, T., Mikawa, S., Hirai, H., 2000. Disruption of AMPA receptor GluR2 clusters following long-term depression induction in cerebellar Purkinje neurons. EMBO J. 19, 2765–2774.

Matsuzaki, Y., Oue, M., Hirai, H., 2014. Generation of a neurodegenerative disease mouse model using lentiviral vectors carrying an enhanced synapsin I promoter. J. Neurosci. Methods 223, 133–143.

Matsuzaki, Y., Konno, A., Mochizuki, R., Shinohara, Y., Nitta, K., Okada, Y., Hirai, H., 2018. Intravenous administration of the adeno-associated virus-PHP.B capsid fails to upregulate transduction efficiency in the marmoset brain. Neurosci. Lett. 665, 182–188.

Mieda, T., Suto, N., Iizuka, A., Matsuura, S., Iizuka, H., Takagishi, K., Nakamura, K., Hirai, H., 2016. Mesenchymal stem cells attenuate peripheral neuronal degeneration in spinocerebellar ataxia type 1 knockin mice. J. Neurosci. Res. 94, 246–252.

Mitsumura, K., Hosoi, N., Furuya, N., Hirai, H., 2011. Disruption of metabotropic glutamate receptor signalling is a major defect at cerebellar parallel fibre-Purkinje cell synapses in staggerer mutant mice. J. Physiol. 589, 3191–3209.

Miyake, K., Miyake, N., Yamazaki, Y., Shimada, T., Hirai, Y., 2012. Serotype-independent method of recombinant adeno-associated virus (AAV) vector production and purification. J. Nippon. Med. Sch. 79, 394–402.

Nitta, K., Matsuzaki, Y., Konno, A., Hirai, H., 2017. Minimal Purkinje cell-specific PCP2/L7 promoter virally available for rodents and non-human primates. Mol. Ther. Methods Clin. Dev. 6, 159–170.

Notartomaso, S., Zappulla, C., Biagioni, F., Cannella, M., Bucci, D., Mascio, G., Scarselli, P., Fazio, F., Weisz, F., Lionetto, L., Simmaco, M., Gradini, R., Battaglia, G., Signore, M., Puliti, A., Nicoletti, F., 2013. Pharmacological enhancement of mGlu1 metabotropic glutamate receptors causes a prolonged symptomatic benefit in a mouse model of spinocerebellar ataxia type 1. Mol. Brain. 6, 48.

Orr, H.T., Chung, M.Y., Banfi, S., Kwiatkowski Jr., T.J., Servadio, A., Beaudet, A.L., McCall, A.E., Duvick, L.A., Ranum, L.P., Zoghbi, H.Y., 1993. Expansion of an unstable trinucleotide CAG repeat in spinocerebellar ataxia type 1. Nat. Genet. 4, 221–226.

Sarachana, T., Hu, V.W., 2013. Genome-wide identification of transcriptional targets of RORA reveals direct regulation of multiple genes associated with autism spectrum disorder. Mol. Autism. 4, 14.

Serra, H.G., Duvick, L., Zu, T., Carlson, K., Stevens, S., Jorgensen, N., Lysholm, A., Burright, E., Zoghbi, H.Y., Clark, H.B., Andresen, J.M., Orr, H.T., 2006. RORalpha-mediated Purkinje cell development determines disease severity in adult SCA1 mice. Cell 127, 697–708.

Shuvaev, A.N., Hosoi, N., Sato, Y., Yanagihara, D., Hirai, H., 2017. Progressive impairment of cerebellar mGluR signalling and its therapeutic potential for cerebellar ataxia in spinocerebellar ataxia type 1 model mice. J. Physiol. 595, 141–164.

Sidman, R.L., Lane, P.W., Dickie, M.M., 1962. Staggerer, a new mutation in the mouse affecting the cerebellum. Science 137, 610–612.

Suto, N., Mieda, T., Iizuka, A., Nakamura, K., Hirai, H., 2016. Morphological and functional attenuation of degeneration of peripheral neurons by mesenchymal stem cell-conditioned medium in spinocerebellar ataxia type 1-knock-in mice. CNS. Neurosci. Ther. 22, 670–676.

Takechi, Y., Mieda, T., Iizuka, A., Toya, S., Suto, N., Takagishi, K., Nakazato, Y., Nakamura, K., Hirai, H., 2013. Impairment of spinal motor neurons in spinocerebellar ataxia type 1-knock-in mice. Neurosci. Lett. 535, 67–72.

Takeo, Y.H., Kakegawa, W., Miura, E., Yuzaki, M., 2015. RORalpha regulates multiple aspects of dendrite development in cerebellar purkinje cells In Vivo. J. Neurosci. 35, 12518–12534.

Torashima, T., Koyama, C., Iizuka, A., Mitsumura, K., Takayama, K., Yanagi, S., Oue, M., Yamaguchi, H., Hirai, H., 2008. Lentivector-mediated rescue from cerebellar ataxia in a mouse model of spinocerebellar ataxia. EMBO Rep. 9, 393–399.

Wang, Y., Kumar, N., Nuhant, P., Cameron, M.D., Istrate, M.A., Roush, W.R., Griffin, P.R., Burris, T.P., 2010. Identification of SR1078, a synthetic agonist for the orphan nuclear receptors RORalpha and RORgamma. ACS Chem. Biol. 5, 1029–1034.

Wang, Y., Billon, C., Walker, J.K., Burris, T.P., 2016. Therapeutic effect of a synthetic RORalpha/gamma agonist in an animal model of autism. ACS Chem. Neurosci. 7, 143–148.

Yamada, M., Sato, T., Tsuji, S., Takahashi, H., 2008. CAG repeat disorder models and human neuropathology: similarities and differences. Acta Neuropathol. 115, 71–86.